Supplement of Atmos. Chem. Phys., 24, 7001–7012, 2024
https://doi.org/10.5194/acp-24-7001-2024-supplement

Atmospheric Chemistry and Physics
Open Access

Supplement of

Technical note: Determining chemical composition of atmospheric single particles by a standard-free mass calibration algorithm

Shao Shi et al.

Correspondence to: Jinghao Zhai (zhaijh@sustech.edu.cn) and Xin Yang (yangx@sustech.edu.cn)

Contents

Section S1. The single particle mass spectrometer used in this study.

This study employed a state-of-the-art single particle aerosol mass spectrometer with high performance (HP-SPAMS, Hexin Instrument Co., Ltd.) to investigate the chemical composition of individual particles. (Du et al., 2024; Li, 2011) Particles were directed into an aerodynamic focusing lens and propelled at velocities dictated by their size. (Carson et al., 1995; Clemen et al., 2020) The vacuum aerodynamic diameter of each particle was then determined by calculating the time delay detected by two continuous lasers (Nd: YAG, 532 nm) oriented at right angles to each other. Particles are then sequentially ionized by laser desorption/ionization (LDI) technique. (Du et al., 2024; Peacock et al., 2017) Within the ion source region, particles triggered a pulsed desorption/ionization laser (Nd: YAG, 266 nm), generating ion fragments. The resulting ions fly under the force of accelerating potential in a TOF-MS. (Murray et al., 2013) For each particle, both positive and negative mass spectra were recorded using a bipolar time-of-flight mass spectrometer (Fig. S1). The raw *m/z* are calculated by TOF data with predetermined parameters of the TOF-MS, e.g., length of flight path and voltage of the accelerating potential.

The initial positions of ions before flight in the TOF-MS are deviated resulting from the focusing limit of AFL, leading to shifts in the flight path and the accelerating potential from the designed parameters (Fig. 1b), and consequently, a drift in the flight time and the corresponding *m/z*. (Dienes, 2003) Since the deviation is uncertain for each particle, specific coefficients are required in the calibration function for individual particles. (Chen et al., 2020; Clemen et al., 2020) Moreover, studies have shown that the inhomogeneity of ionizing laser could also influence the mass measurement. (Wenzel and Prather, 2004)

The power of the desorption/ionization laser was set to ~0.6 mJ/pulse in this study. To ensure accurate size determination, the aerodynamic diameter measurements were

calibrated using monodisperse polystyrene latex spheres (Nanosphere size standards) with known diameters ranging from 0.05 to 5.0 μm. To improve data quality, all acquired single particle mass spectra were subjected to a filtering process that set a minimum signal threshold of 50 mV above the baseline for each *m/z* within the range of ± (1-500) Th.

The relation between *m/z* and mass resolution (R_m) is described in the empirical equation (S1). (Du et al., 2024)The equation is used for the localization of our algorithm.

$$R_m = -0.04549(\mathrm{m}/z)^2 + 22.98\frac{m}{z} + 199.6 \quad \text{(S1)}$$

The $\boldsymbol{m/z}_{\mathrm{r}}$ was converted from TOF data $\boldsymbol{t}$ using equation (S2), with coefficients provided in the following table, the unit of TOF is ns.

$$\boldsymbol{m/z}_{\mathrm{r}} = \left(\frac{\boldsymbol{t} - t_0}{m_0}\right)^2 \quad \text{(S2)}$$

polarity	t_0	m_0
positive	-714.829468	1216.546875
negative	-714.993408	1209.078735

Section S2. Detailed description of traits in the prototype.

It is essential to choose traits to establish the prototype to ensure accurate calibration of mass spectrometer spectra. Prototype is a concept borrowed from statistic machine learning, but the mechanism of prototype in our algorithm is more like the reward defined in reinforcement learning. (Hastie et al., 2009)

For instance, in the S_r to be calibrated, if a peak is observed around 51 Th, and the calibration target is mass deviation less than 0.025 Th, it remains uncertain whether the exact value is 50.95 Th (V^+) or 51.00 Th ($C_4H_3^+$) before calibration (in atmospheric aerosols, V^+ and $C_4H_3^+$ are only choices for a reasonable peak around 51 Th). However, suppose a calibration attempt aligns it to 51.00 Th, and simultaneously, a minor peak at 52.00 Th adheres to the isotopic distribution of $C_4H_3^+$ (i.e., p(51.00 Th): p(52.05 Th) = 1: 0.43). In that case, this peak is likely corresponding to 51.00 Th ($C_4H_3^+$). Conversely, if it is calibrated to 50.95 Th and satisfies the monoisotopic characteristic of V^+, it could be identified as 50.95 (V^+). Additionally, if prominent peaks are both observed around 51 Th and 67 Th and a series of organic signals (e.g., C_mH_n signals) is absent, these peaks may be identified as V^+ (50.95 Th) and VO^+ (66.95 Th), respectively. The isotopic distributions thus serve as traits of exact spectra. Any calibration attempt that relocates the peak contrary to these distributions would be deemed incorrect. Trait matching is considered specific because a peak matched to more than one trait is in low probability. Although it is easy to determine whether a trait is not possessed/matched by a spectrum, it is hard to judge whether a trait is truly possessed (definitely positive) by a spectrum. Once the trait is matched, it is essential to assess the behavior of S_t across the entire prototype database using the value function before confirming a trait is truly positive. Therefore, the traits that matched are only considered truly positive in S_{opt}.

Consider another example spectrum containing only C^+ (12.00 Th), C_2^+ (24.00 Th), C_3^+ (36.00 Th), C_4^+ (48.00 Th), C_5^+ (60.00 Th), and $C_4H_3^+$, and these peaks are collected in the prototype database. Although this information is unknown before calibration, we can evaluate any calibration attempt by matching these *m/z*. The optimal calibration attempt, S_{opt}, would align all six peaks to their respective theoretical positions by the prototype, resulting in peaks at 12.00 Th, 24.00 Th, 36.00 Th, 48.00 Th, 60.00 Th, and 51.00 T. Any S_t calibrate these peaks to other *m/z* position is not the optimal calibration.

A special type of traits is isolate ions because the trait matching of this type is certain. For instance, if we observed the presence of a peak around 12 Th. Given the mass deviation range (± 0.1 Th at 12 Th), the only valid theoretical choice for its value would be 12.00 Th (C^+) in atmospheric aerosol samples. Consequently, any calibration attempt that relocates this peak to a position other than 12.00 Th is miscalibration. Additionally, if a small peak is observed around 13 Th, along with a strong peak at 12 Th and following the isotope distribution of carbon, the assertion is further confirmed.

Section S3. Simplified pseudocode of the algorithm.

Standard-free calibration Algorithm: calibration core

Input: The raw mass spectrum *raw*, the prototype database *ptt*, the θ space *space*.

Output: The optimal calibrated spectrum *opcalied.*

```
maxValue = 0
optCoef = 0
for θ in space
    S.mz = f(raw.mz, θ)
    thisValue = 0
    for Ti in ptt
        thisValue = thisValue + Ti.wi * match(Ti, S)
    end for
    if thisValue > maxValue then
        maxValue = thisValue
        optCoef = θ
        opcalied = S
    end if
end for
return opcalied
```

The core algorithm of the match function (equation (3)) could be a modification of binary search, or positive matrix factorization. In this study, the match function adopted a variation of binary search with a complexity of *O(nlogn)* to the number of peaks in the mass spectrum. Tolerance of mass difference was set to the resolving ability for the fuzzy matching of *m/z*. In addition, *f(raw, θ)* is the mass calibration function mentioned in equation (1), and *value* is the function in equation (2).

Section S4. Details about determining the chemical species at ~51 Th.

When assigning the corresponding chemicals of peaks at 50.95 Th, all possibilities whose exact *m/z* in 50.925-50.975 Th should be checked. Here, we listed all species at ~50.95 Th in Table S1, and compared our result with the NIST database and the PubChem database. (Linstrom et al., 2024; Kim et al., 2023)

Table S1. Possible ions around 50.95 Th under 500-ppm accuracy.

Ion	Exact *m/z* (Th)	NIST	PubChem
V^+	50.9434	Have data	Have data
SF^+	50.9699	Have data	Have data
ClO^+	50.9632	No data	No data
TiH_3^+	50.9709	No data	No data

The SF^+ ion is unstable and rarely encountered in the atmosphere. Instead, the existence of V^+ in atmospheric aerosols has been widely reported. (Ault et al., 2010; Zhai et al., 2023; Wang et al., 2023; Passig et al., 2020, 2021; Anders et al., 2023) Therefore, we consider V^+ to be the corresponding species at 50.95 Th. Additionally, most 50.95-Th-containing spectra also contain peaks at 66.95 Th (the exact mass of VO^+), indicating the assignment of V^+ at 50.95 Th is self-consistent.

Possible ions around 51.00 Th under 500-ppm accuracy (50.925-50.975 Th) are listed below (Table S2).

Table S2. Possible ions around 51.00 Th under 500-ppm accuracy.

Ion	Exact *m/z* (Th)	NIST	PubChem
AlC_2^+	50.9810	No data	No data
$CBSi^+$	50.9857	No data	No data
ClH_2N^+	50.9870	Have data	No data
$LiOSi^+$	50.9872	No data	No data
FO_2^+	50.9877	No data	No data

H_3OS^+	50.9900	No data	Have data
$H_3Mg_2^+$	50.9930	No data	No data
CH_4Cl^+	50.9996	No data	Have data
CHF_2^+	51.0041	Have data	Have data
$CLiO_2^+$	51.0053	No data	No data
C_3HN^+	51.0104	Have data	Have data
H_5NS^+	51.0137	No data	No data
$C_4H_3^+$	51.0229	Have data	Have data

The existence of most of these species has not been reported in previous studies. Elements in some species are in trace amounts in the atmosphere, including B, F, and Li. Species like ClH_2N^+ have more than one heteroatom, which makes the occurrence of these species in the mass spectra lower than simple species that contain only C, H, and N. For these reasons, we only consider $C_4H_3^+$ and C_3NH^+ as candidates at 51.00 Th. As shown in Figure 5 and Figure S4, spectra containing 51.00 Th also contain peaks at 12.00 Th (C^+), 36.00 Th (C_3^+), 37.00 Th (C_3H^+), 38.00 Th ($C_3H_2^+$), 39.00 Th ($C_3H_3^+$), 43.05 Th ($C_3H_7^+$), and 50.00 Th ($C_4H_2^+$). The combination of all these species is consistent with the distribution pattern of $C_mH_n^+$ fragments. Therefore, we assign 51.00 Th as $C_4H_3^+$ in our study. Further, the existence of $C_4H_3^+$ has been reported in previous studies (including ambient studies).(Zhai et al., 2023; Wang et al., 2023; Du et al., 2024; Xiao et al., 2018)

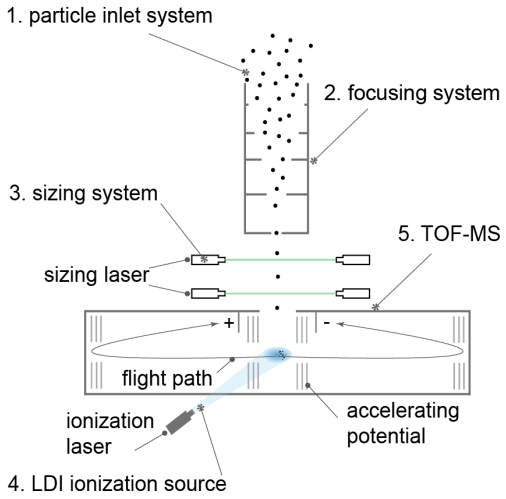

Figure S1. Simplified operational mechanism of the HP-SPAMS. Particle sequentially goes through stage 1-5 to generate a raw TOF spectrum.

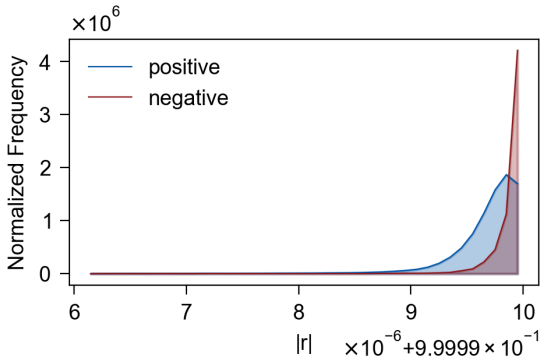

130

131 **Figure S2.** Histogram of $|r|$ for positive and negative spectra. The histogram of $|r|$ values
132 for positive and negative spectra demonstrates that all the calibrations result in $|r|$ values
133 greater than 0.999996. Shaded areas are summed to 1.

134

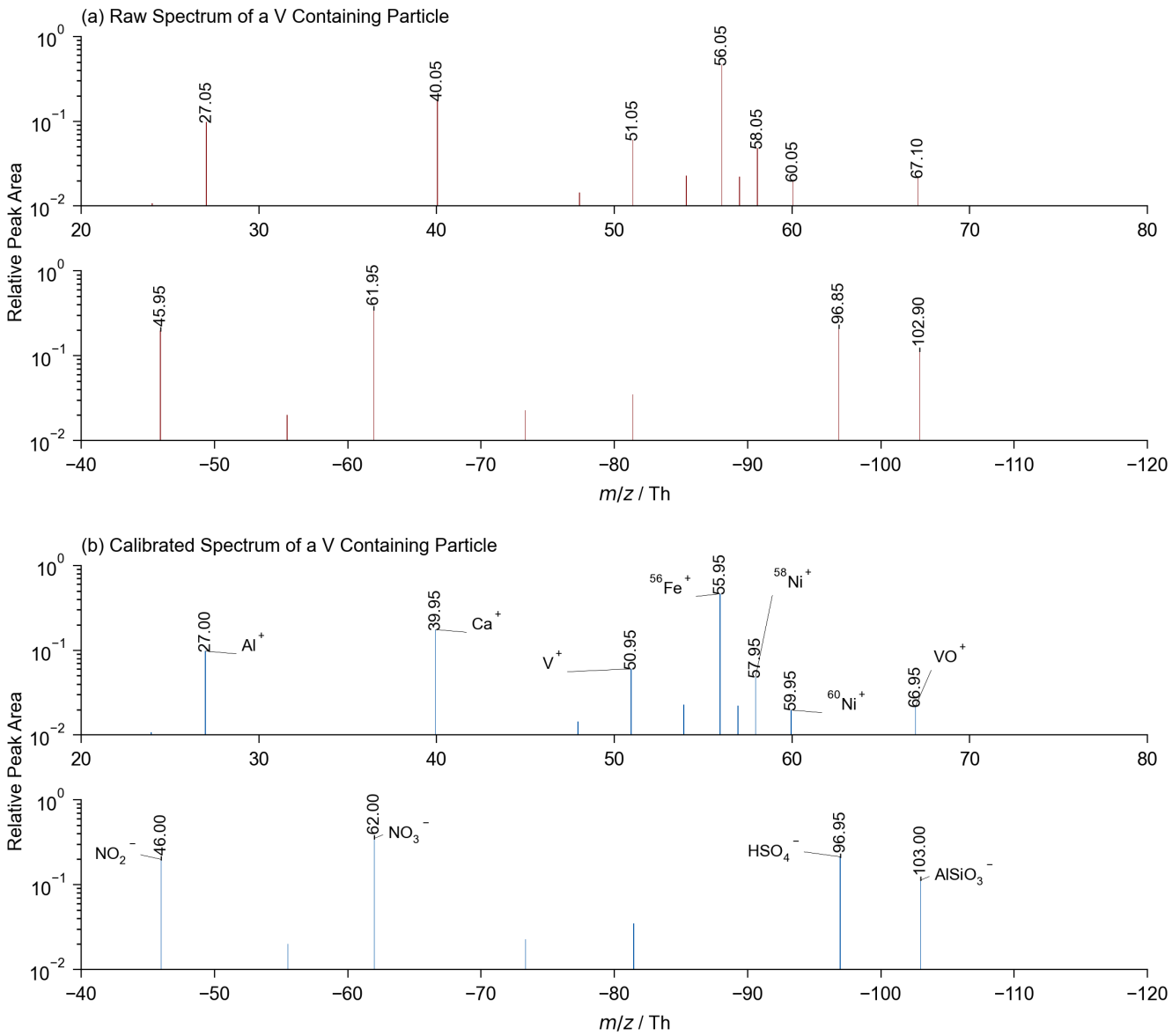

135 **Figure S3.** Example of raw (a) and calibrated (b) single-particle mass spectra of a typical

136 vanadium (V) containing particle.

137

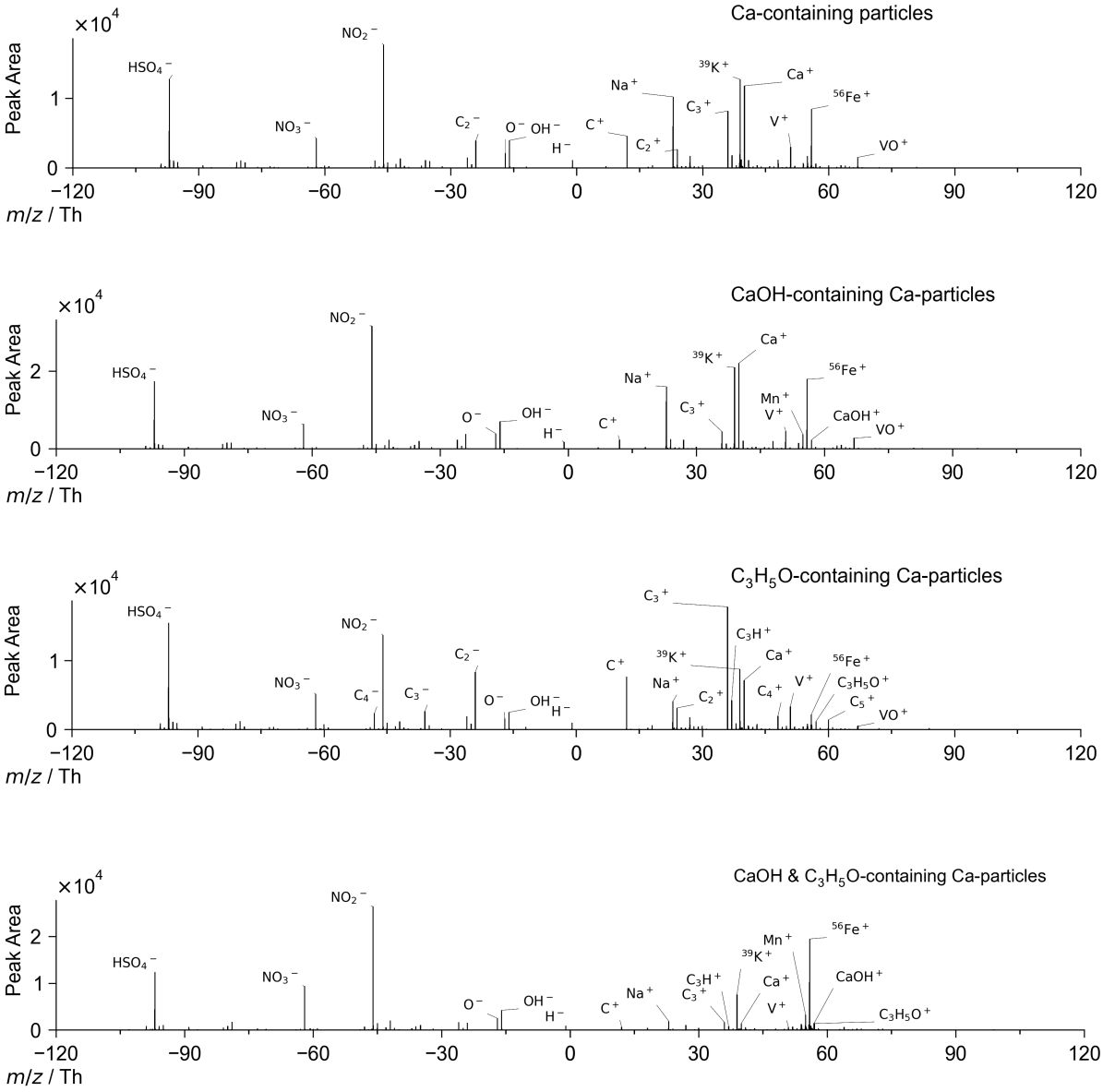

Figure S4. Averaged mass spectra of Ca^+-containing, Ca^+ & $CaOH^+$(only)-containing, Ca^+ & $C_3H_5O^+$ (only)-containing, and Ca^+ & $CaOH^+$ & $C_3H_5O^+$-containing particles.

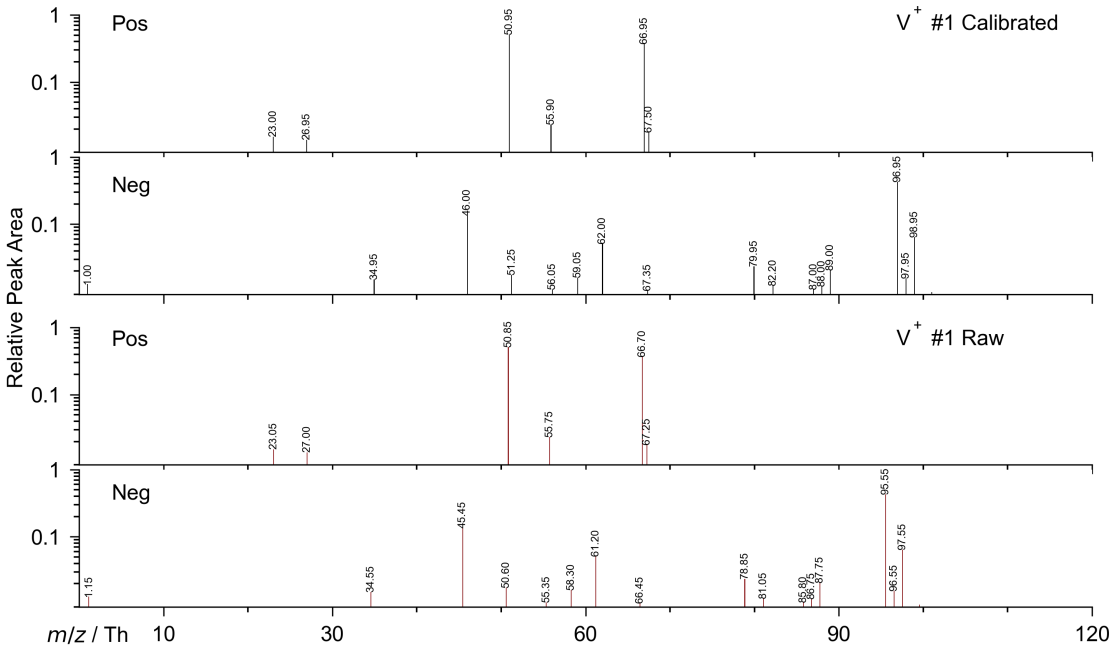
Pos
V+ #1 Calibrated
Neg
Pos
V+ #1 Raw
Neg
Relative Peak Area
m/z / Th
10
30
60
90
120

145

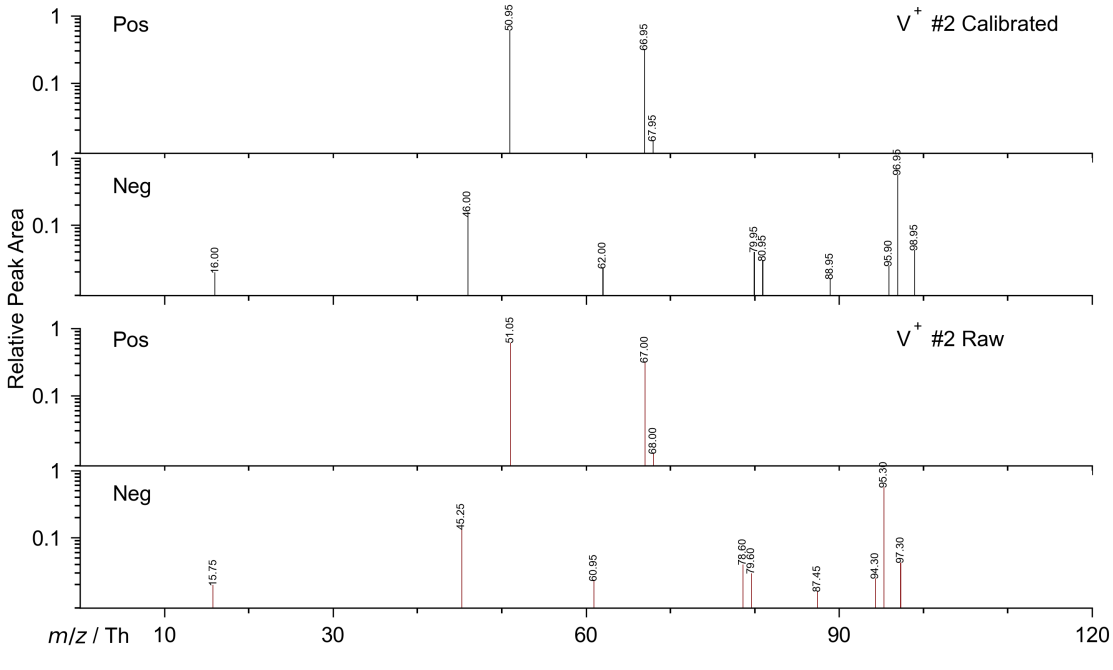
Pos
V+ #2 Calibrated
Neg
Pos
V+ #2 Raw
Neg
Relative Peak Area
m/z / Th
10
30
60
90
120

146

147

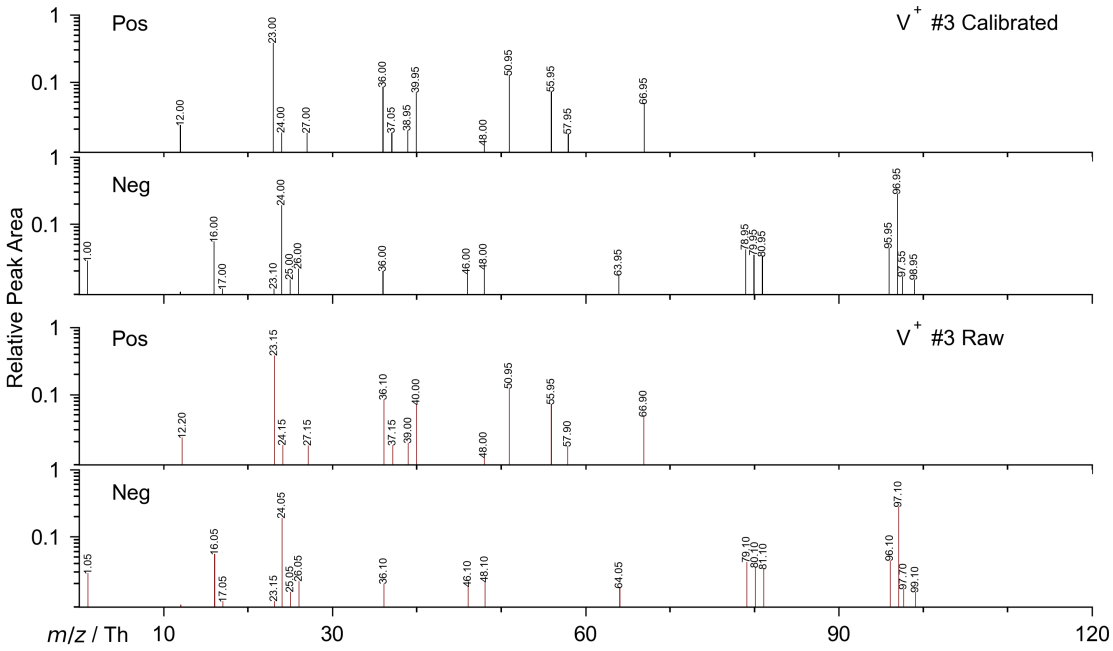
Pos
V+ #3 Calibrated
Neg
Pos
V+ #3 Raw
Neg
Relative Peak Area
m/z / Th
10
30
60
90
120

148

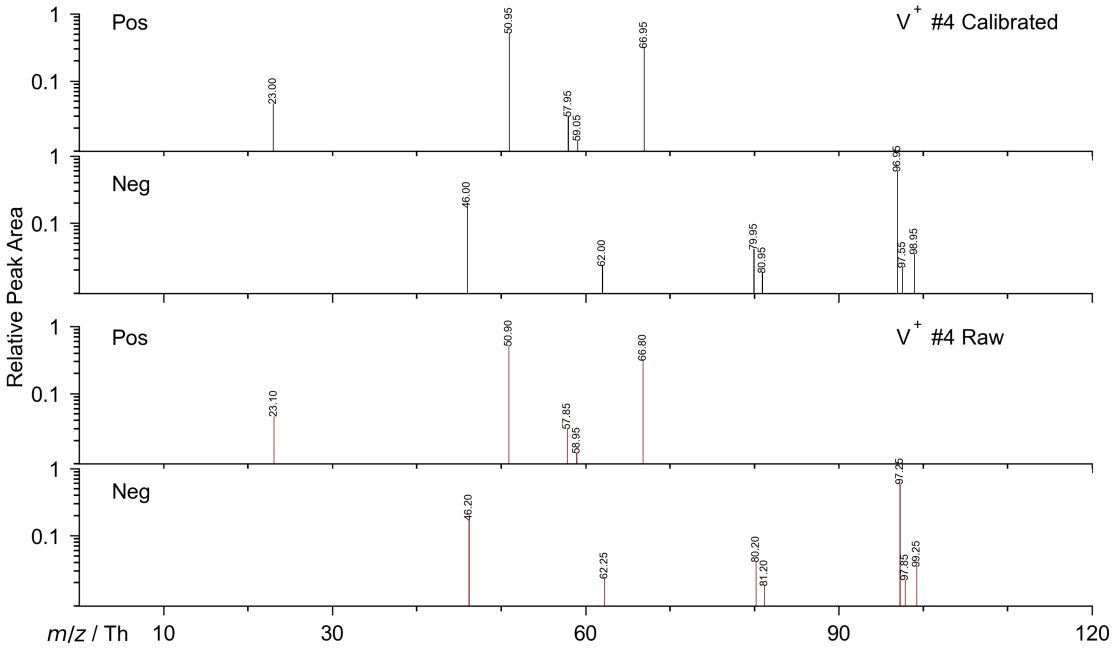
Pos
V+ #4 Calibrated
Neg
Pos
V+ #4 Raw
Neg
Relative Peak Area
m/z / Th
10
30
60
90
120

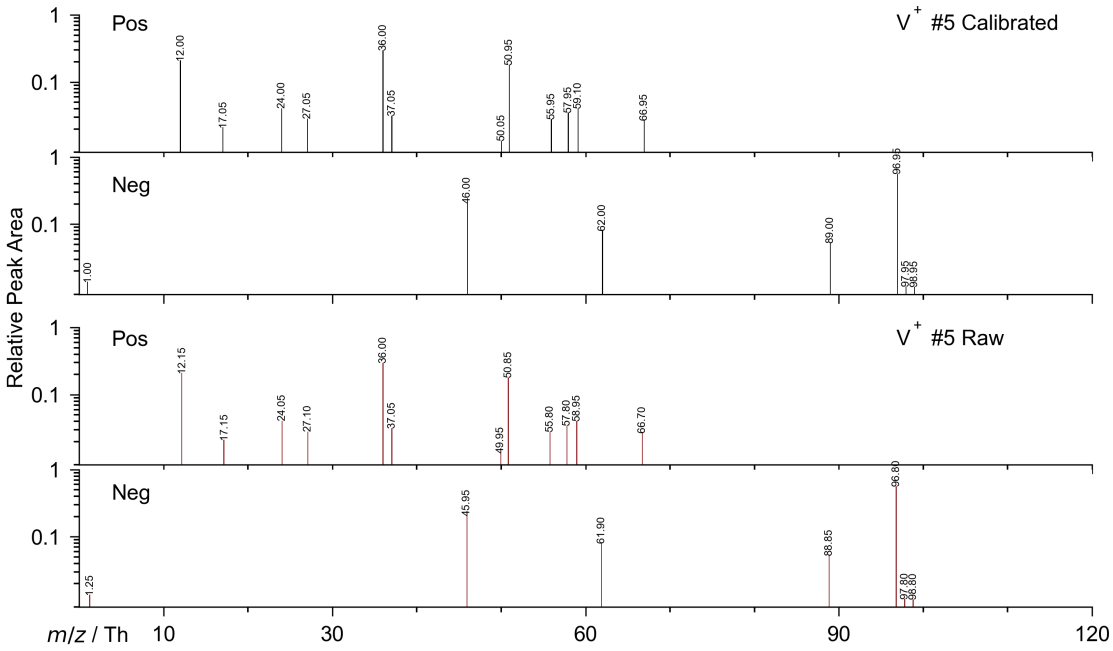
Pos
V+ #5 Calibrated
Neg
Pos
V+ #5 Raw
Neg
Relative Peak Area
m/z / Th
10
30
60
90
120

149

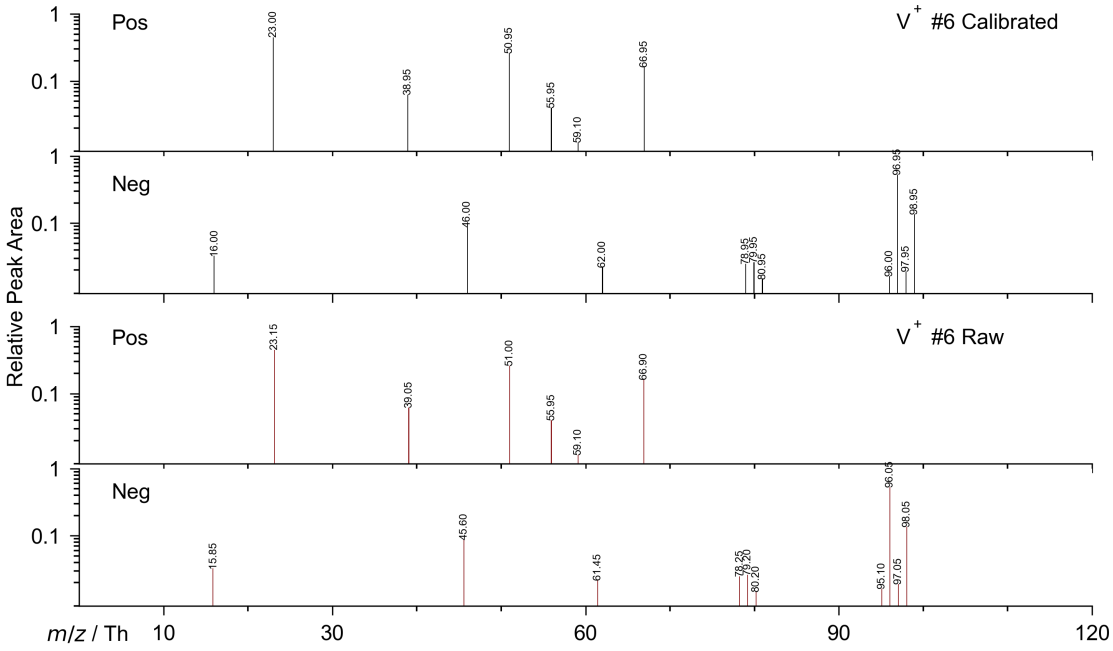
Pos
V+ #6 Calibrated
Neg
Pos
V+ #6 Raw
Neg
Relative Peak Area
m/z / Th
10
30
60
90
120

150

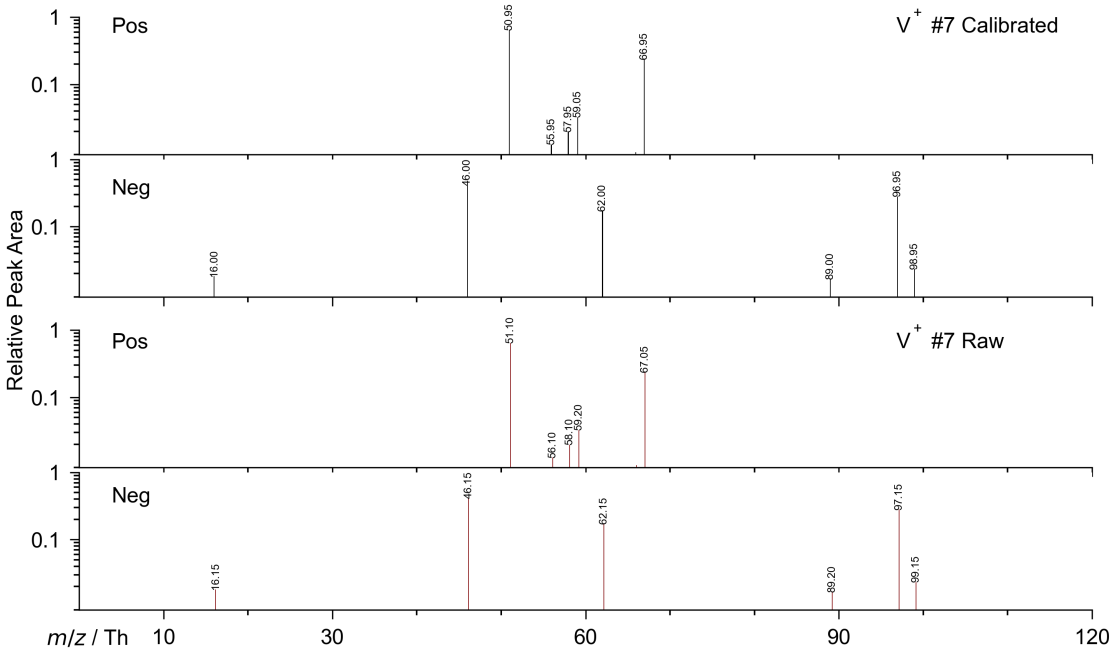
Pos
V+ #7 Calibrated
Neg
Pos
V+ #7 Raw
Neg
Relative Peak Area
m/z / Th
10
30
60
90
120

151

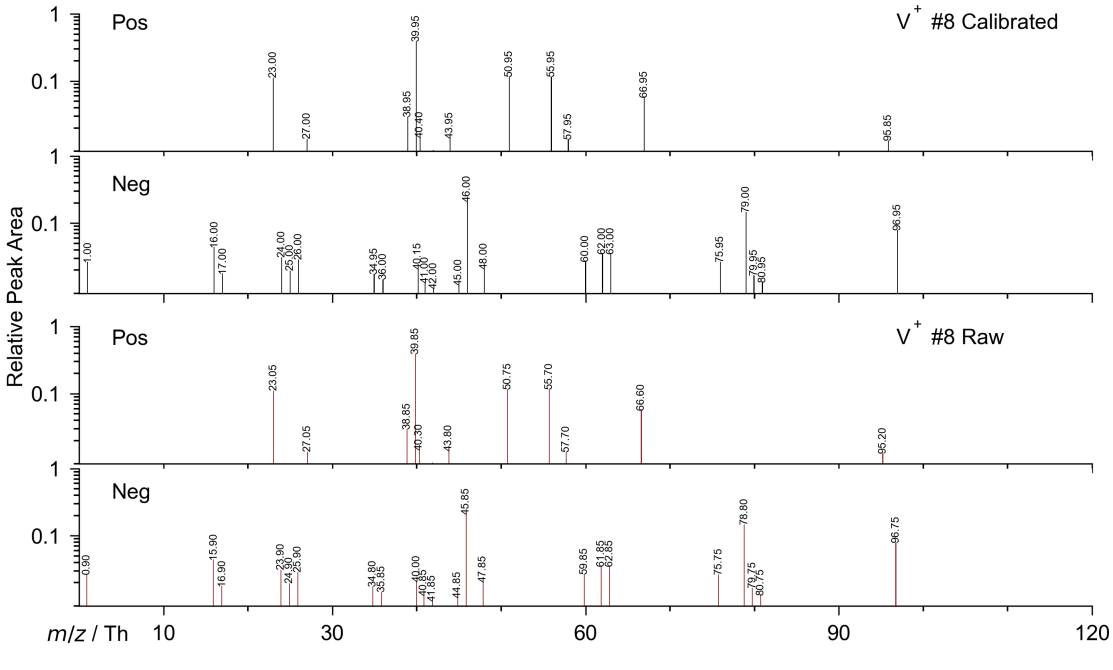
Pos
V+ #8 Calibrated
Neg
Pos
V+ #8 Raw
Neg
Relative Peak Area
m/z / Th
10
30
60
90
120

152

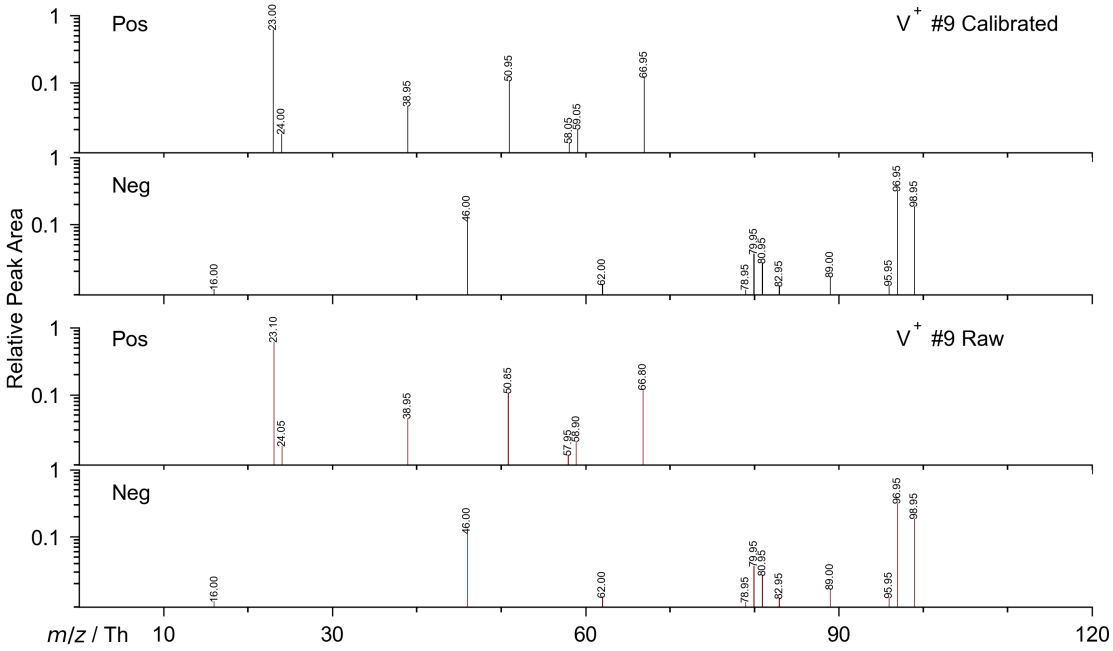
Pos
V+ #9 Calibrated
Neg
Pos
V+ #9 Raw
Neg
Relative Peak Area
m/z / Th
10
30
60
90
120

153

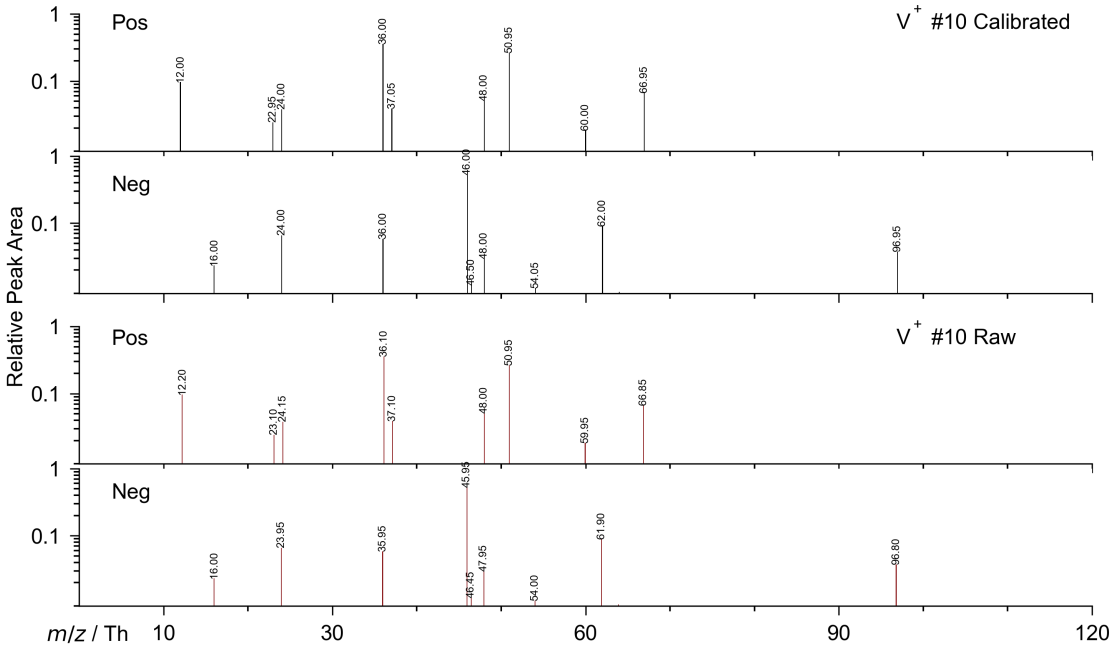
Pos
V+ #10 Calibrated
Neg
Pos
V+ #10 Raw
Neg
Relative Peak Area
m/z / Th
10
30
60
90
120

154

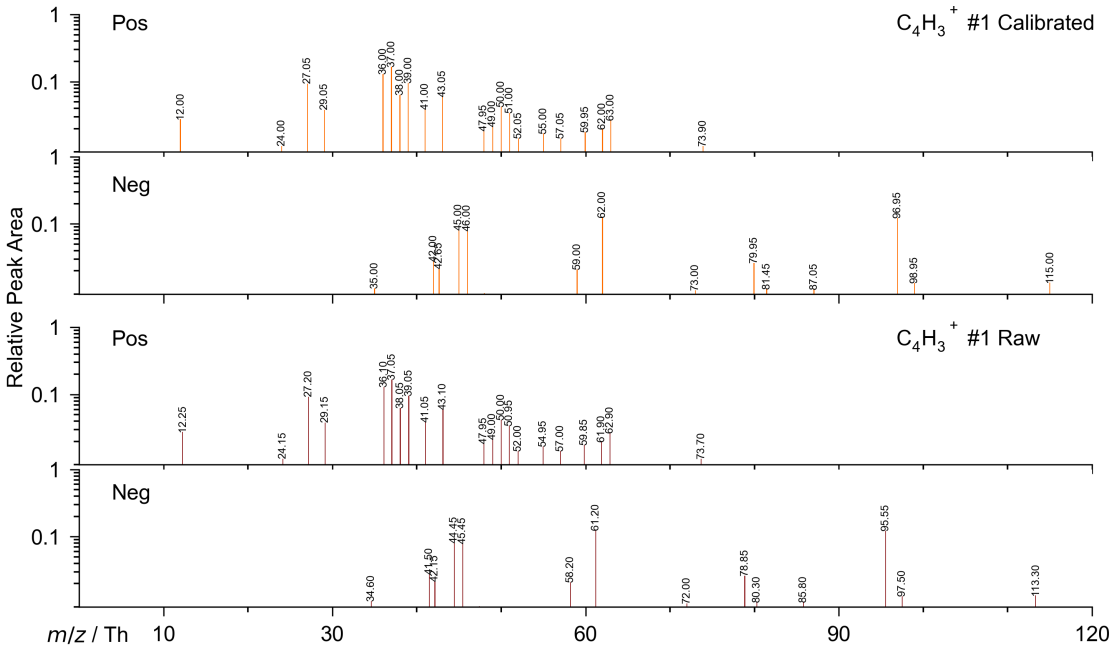
Pos
$C_4H_3^+$ #1 Calibrated
Neg
Pos
$C_4H_3^+$ #1 Raw
Neg
Relative Peak Area
m/z / Th
10
30
60
90
120

155

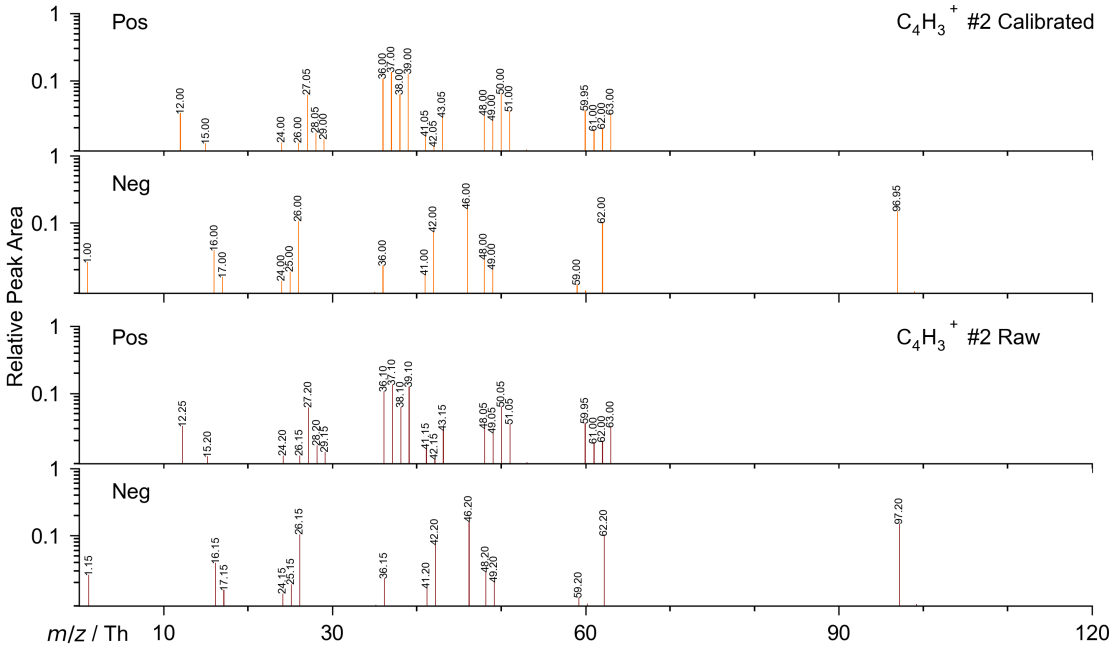
Pos
$C_4H_3^+$ #2 Calibrated
Neg
Pos
$C_4H_3^+$ #2 Raw
Neg
Relative Peak Area
m/z / Th
10
30
60
90
120

156

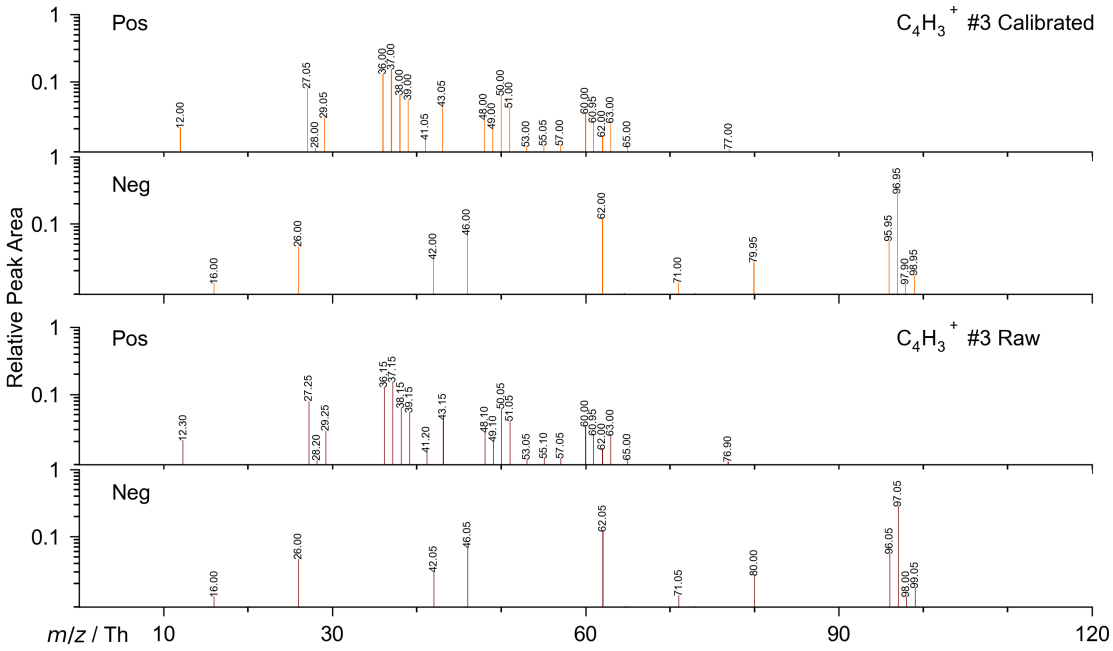
Pos
$C_4H_3^+$ #3 Calibrated
Neg
Pos
$C_4H_3^+$ #3 Raw
Neg
Relative Peak Area
m/z / Th
10
30
60
90
120

157

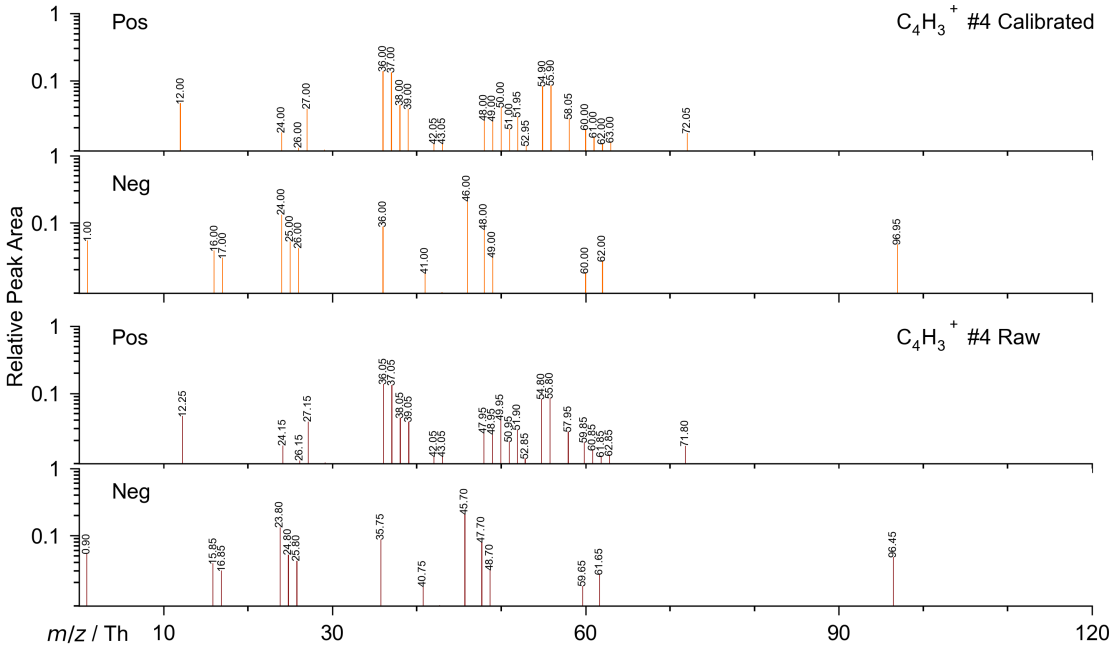
Pos
$C_4H_3^+$ #4 Calibrated
Neg
Pos
$C_4H_3^+$ #4 Raw
Neg
Relative Peak Area
m/z / Th
10
30
60
90
120

158

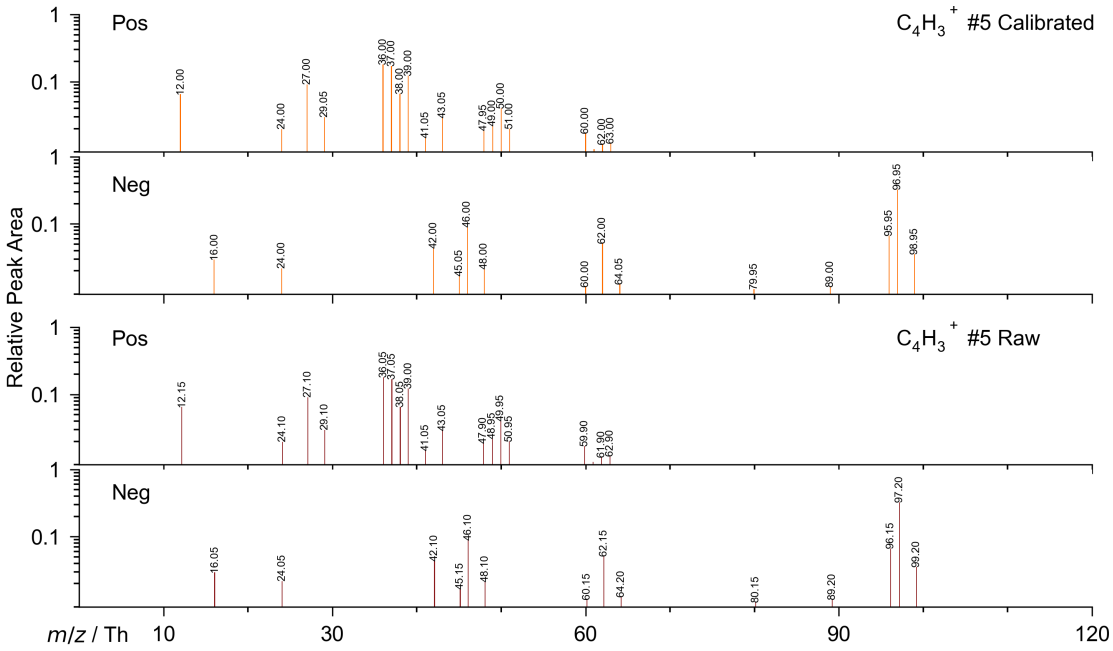
Pos
$C_4H_3^+$ #5 Calibrated
Neg
Pos
$C_4H_3^+$ #5 Raw
Neg
Relative Peak Area
m/z / Th
10
30
60
90
120

159

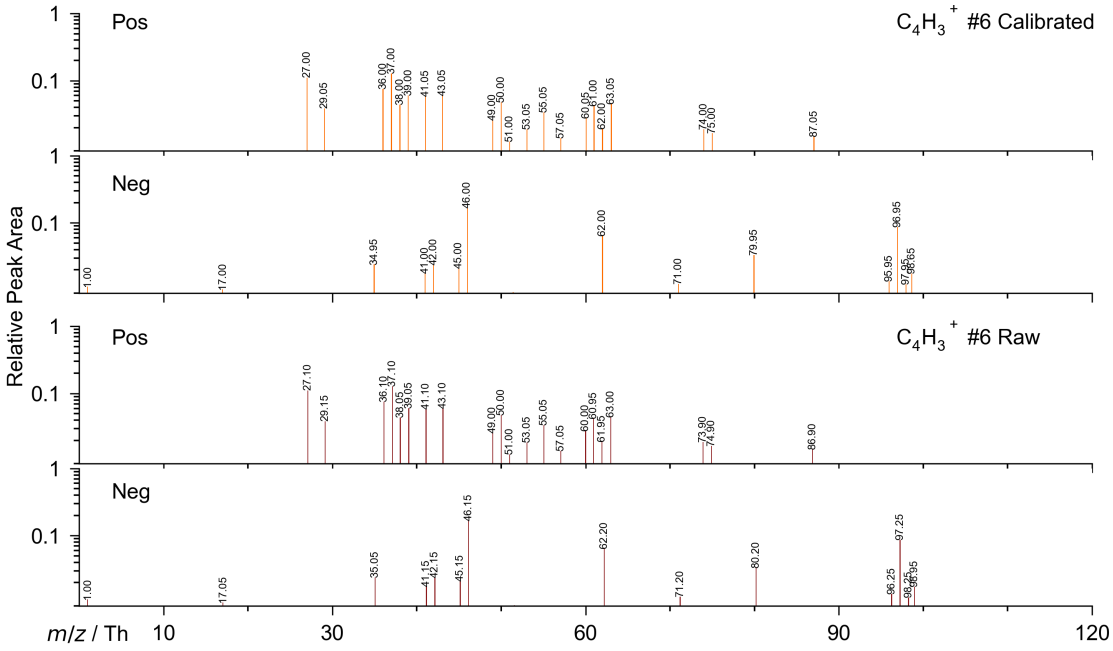
Pos
$C_4H_3^+$ #6 Calibrated
Neg
Pos
$C_4H_3^+$ #6 Raw
Neg
Relative Peak Area
m/z / Th
10
30
60
90
120

160

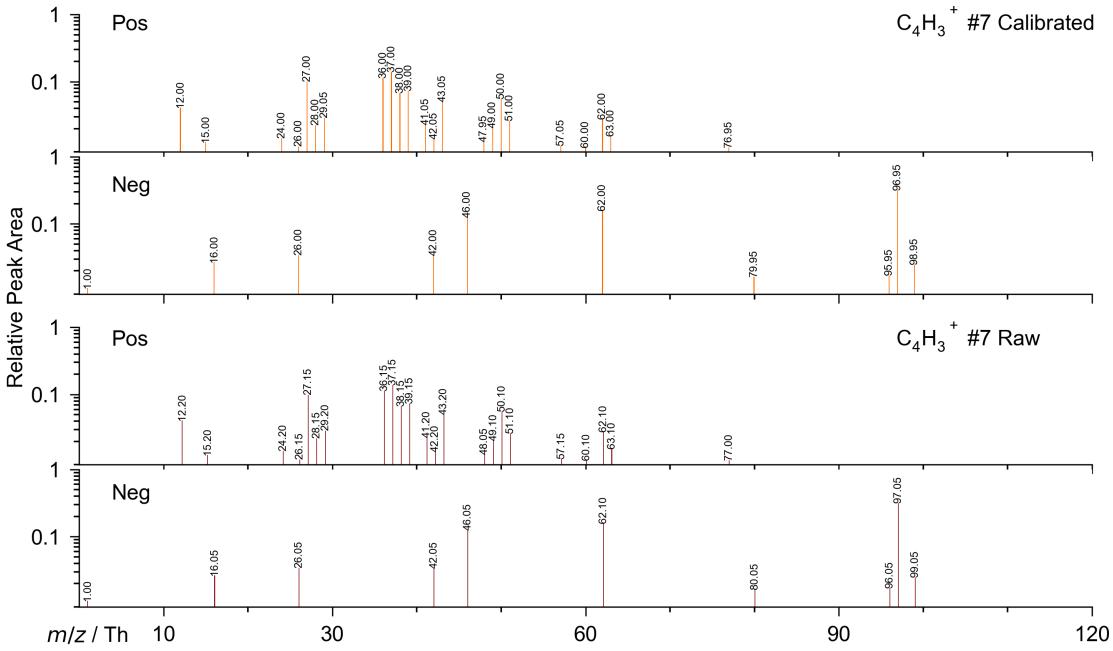
Pos
$C_4H_3^+$ #7 Calibrated
Neg
Pos
$C_4H_3^+$ #7 Raw
Neg
Relative Peak Area
m/z / Th
10
30
60
90
120

161

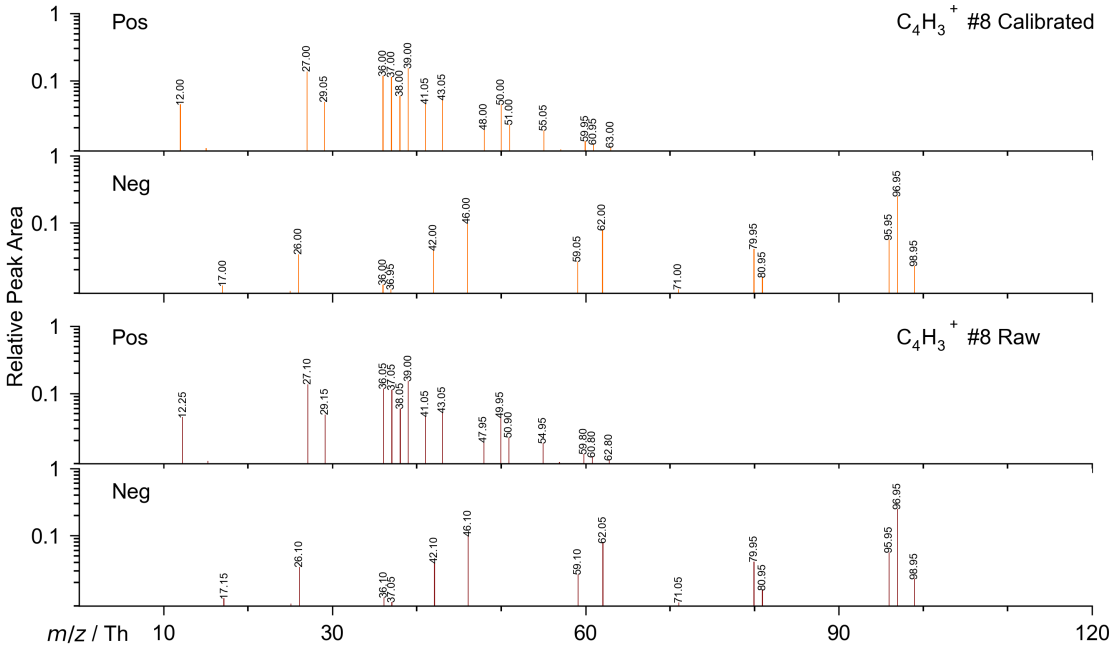
Pos
$C_4H_3^+$ #8 Calibrated
Neg
Pos
$C_4H_3^+$ #8 Raw
Neg
Relative Peak Area
m/z / Th
10
30
60
90
120

162

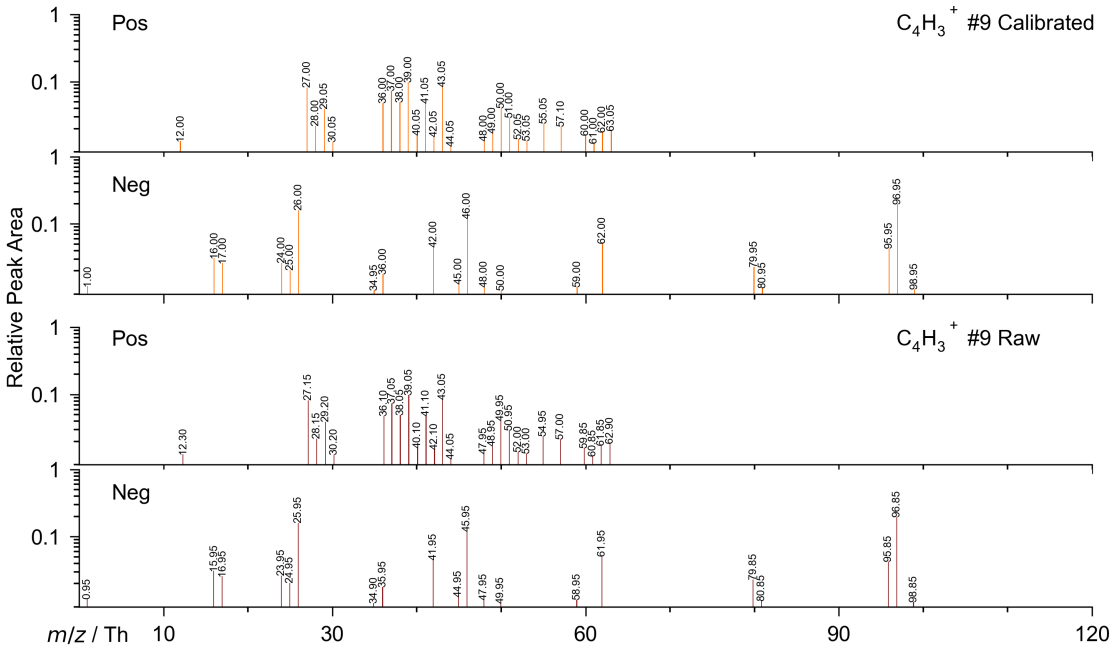

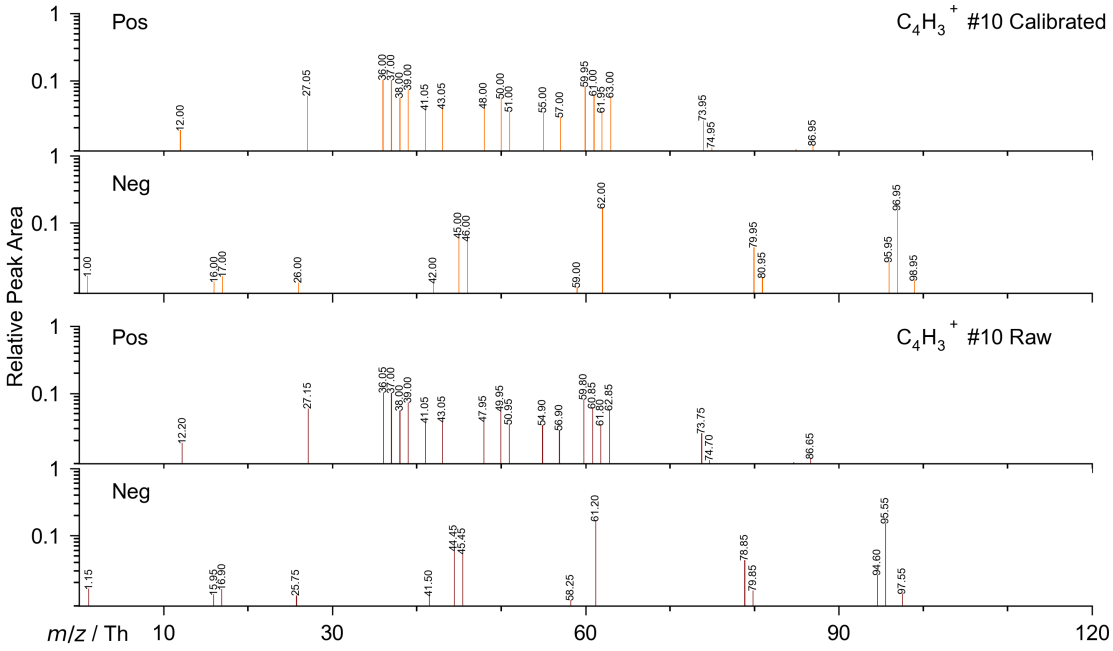

Figure S5. Examples of calibrated and raw single-particle mass spectra of V^+-containing particles and $C_4H_3^+$-containing particles. The spectra are randomly chosen from the two particle groups.

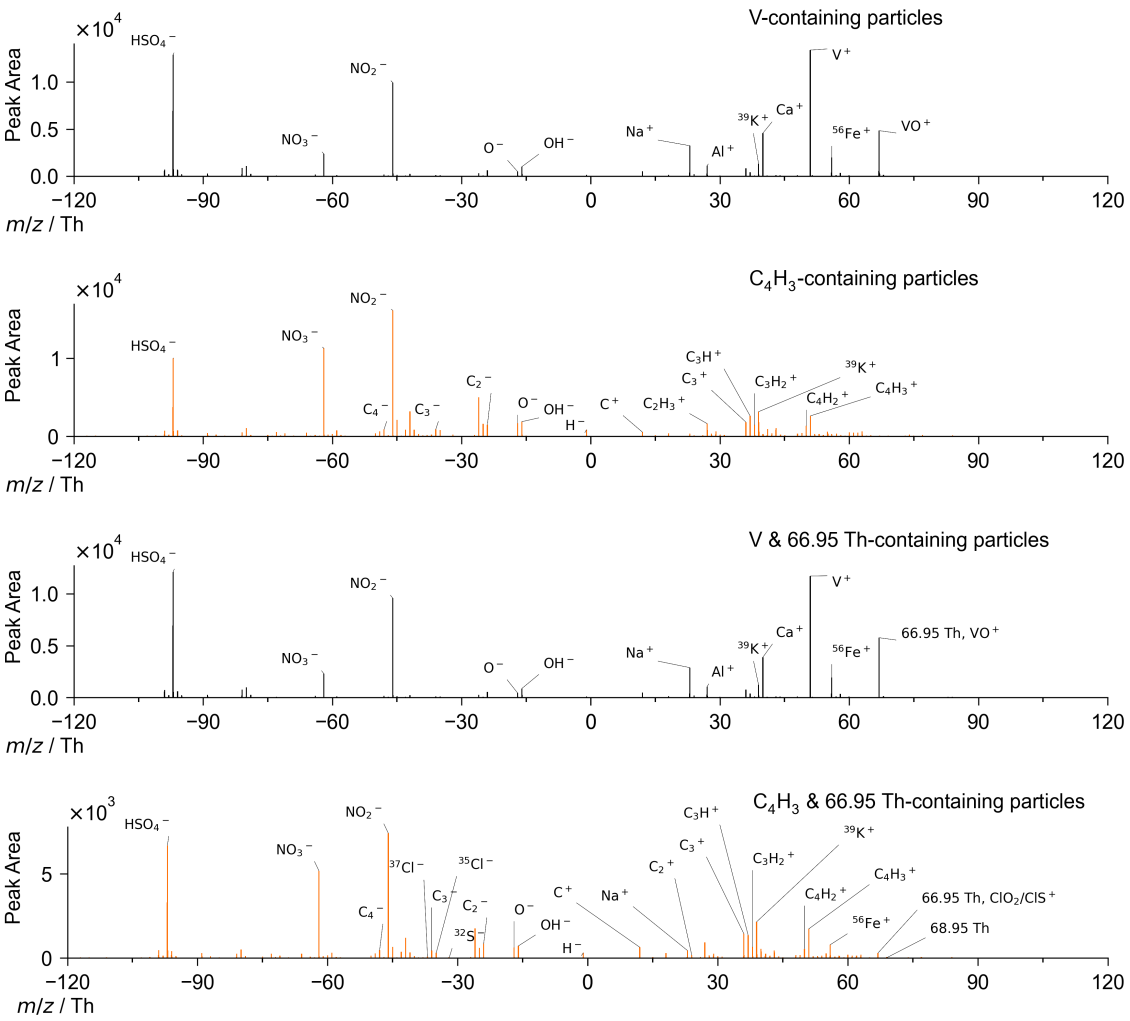

Figure S6. Averaged mass spectra of V^+-containing and $C_4H_3^+$-containing particles and V^+-containing and $C_4H_3^+$-containing particles that contain 66.95 Th signal. The average peak area of 66.95 Th in the V^+ group is larger than 5,500, in the $C_4H_3^+$ group the average peak area of 66.95 Th is ~300 on average. The ratio of peak area of ~51 Th to 66.95 Th in the two groups is 2.03 and 5.79, separately. The peak-area ratio of 66.95 Th : 68.95 Th in "C_4H_3 & 66.95 Th" spectrum is 1 : 0.25 (300.10 : 72.40), the slight deviation from theoretical value (1 : 0.32) is likely due to the approaching of the signal-noise threshold (50), in the negative spectrum, the distribution of Cl^- isotopes is -34.95 Th : -36.95 Th = 1 : 0.28 (306.92 : 87.32).

Table S3. Accuracy and resolution required for separating easily confused ions typically encountered in aerosol research (50% separation).

Ion pair	Isotopic *m/z* (Th)	*Δm/z* (Th)	Accuracy (ppm)	Resolution (FWHM)
Mg^+/C_2^+	23.9845/23.9995	0.0150	625.0	2400
$Al^+/C_2H_3^+$	26.9810/27.0229	0.0419	1551	967.5
$Ca^+/NaOH^+$	39.9620/39.9920	0.0300	750.7	1998
K^+/C_2NH^+	38.9631/39.0104	0.0473	1212	1237
Ti^+/C_4^+	47.9474/ 47.9995	0.0521	1085	1382
$V^+/C_4H_3^+$	50.9434/ 51.0229	0.0795	1558	962.7
$Mn^+/C_3H_3O^+$	54.9375/55.0178	0.0803	1460	1028
$Cu^+/C5H3^+$	62.9290/63.0229	0.0939	1490	1007
Sn^+/C_{10}^+	119.9016/119.9995	0.0979	815.8	1838
SO^-/C_4^-	47.9675/48.0005	0.0330	687.5	2183
Br^-/PO_3^-	78.9189/78.9591	0.0402	509.1	2946

Table S4. The presence of ions in Ca^+-containing particles.

Ion	Count	Fraction / %
Ca^+	910,483	100
$CaOH^+$	252,160	28
$C_3H_5O^+$	79,155	8.7
$CaOH^+$ & $C_3H_5O^+$	5,601	0.62

References

Anders, L., Schade, J., Rosewig, E. I., Kröger-Badge, T., Irsig, R., Jeong, S., Bendl, J., Saraji-Bozorgzad, M. R., Huang, J.-H., Zhang, F.-Y., Wang, C. C., Adam, T., Sklorz, M., Etzien, U., Buchholz, B., Czech, H., Streibel, T., Passig, J., and Zimmermann, R.: Detection of ship emissions from distillate fuel operation via single-particle profiling of polycyclic aromatic hydrocarbons, Environ. Sci.: Atmos., 3, 1134–1144, https://doi.org/10.1039/D3EA00056G, 2023.

Ault, A. P., Gaston, C. J., Wang, Y., Dominguez, G., Thiemens, M. H., and Prather, K. A.: Characterization of the Single Particle Mixing State of Individual Ship Plume Events Measured at the Port of Los Angeles, Environ. Sci. Technol., 44, 1954–1961, https://doi.org/10.1021/es902985h, 2010.

Carson, P. G., Neubauer, K. R., Johnston, M. V., and Wexler, A. S.: On-line chemical analysis of aerosols by rapid single-particle mass spectrometry, J. Aerosol Sci., 26, 535–545, https://doi.org/10.1016/0021-8502(94)00133-J, 1995.

Chen, Y., Kozlovskiy, V., Du, X., Lv, J., Nikiforov, S., Yu, J., Kolosov, A., Gao, W., Zhou, Z., Huang, Z., and Li, L.: Increase of the particle hit rate in a laser single-particle mass spectrometer by pulse delayed extraction technology, Atmos. Meas. Tech., 13, 941–949, https://doi.org/10.5194/amt-13-941-2020, 2020.

Clemen, H.-C., Schneider, J., Klimach, T., Helleis, F., Köllner, F., Hünig, A., Rubach, F., Mertes, S., Wex, H., Stratmann, F., Welti, A., Kohl, R., Frank, F., and Borrmann, S.: Optimizing the detection, ablation, and ion extraction efficiency of a single-particle laser ablation mass spectrometer for application in environments with low aerosol particle concentrations, Atmos. Meas. Tech., 13, 5923–5953, https://doi.org/10.5194/amt-13-5923-2020, 2020.

Dienes, T.: Development, characterization, and refinement of a transportable aerosol time-of-flight mass spectrometer, University of California, Riverside, 2003.

Du, X., Xie, Q., Huang, Q., Li, X., Yang, J., Hou, Z., Wang, J., Li, X., Zhou, Z., Huang, Z., Gao, W., and Li, L.: Development and characterization of a high-performance single-particle aerosol mass spectrometer (HP-SPAMS), Atmos. Meas. Tech., 17, 1037–1050, https://doi.org/10.5194/amt-17-1037-2024, 2024.

Hastie, T., Tibshirani, R., and Friedman, J.: The Elements of Statistical Learning, Springer New York, New York, NY, https://doi.org/10.1007/978-0-387-84858-7, 2009.

Kim, S.; Chen, J.; Cheng, T.; Gindulyte, A.; He, J.; He, S.; Li, Q.; Shoemaker, B. A.; Thiessen, P. A., Yu, B.; Zaslavsky, L.; Zhang, J.; and Bolton, E. E. PubChem 2023

update. Nucleic Acids Res., 51(D1), D1373–D1380. https://doi.org/10.1093/nar/gkac956, 2023.

Linstrom, P. J.; Mallard, W. G.; Eds., NIST Chemistry WebBook, NIST Standard Reference Database Number 69, National Institute of Standards and Technology, Gaithersburg MD, 20899, https://doi.org/10.18434/T4D303, 2024.

Li, L.: Real time bipolar time-of-flight mass spectrometer for analyzing single aerosol particles, Int. J. Mass Spectrom., 2011.

Murray, K. K., Boyd, R. K., Eberlin, M. N., Langley, G. J., Li, L., and Naito, Y.: Definitions of terms relating to mass spectrometry (IUPAC Recommendations 2013), Pure Appl. Chem., 85, 1515–1609, https://doi.org/10.1351/PAC-REC-06-04-06, 2013.

Passig, J., Schade, J., Rosewig, E. I., Irsig, R., Kröger-Badge, T., Czech, H., Sklorz, M., Streibel, T., Li, L., Li, X., Zhou, Z., Fallgren, H., Moldanova, J., and Zimmermann, R.: Resonance-enhanced detection of metals in aerosols using single-particle mass spectrometry, Atmos. Chem. Phys., 20, 7139–7152, https://doi.org/10.5194/acp-20-7139-2020, 2020.

Passig, J., Schade, J., Irsig, R., Li, L., Li, X., Zhou, Z., Adam, T., and Zimmermann, R.: Detection of ship plumes from residual fuel operation in emission control areas using single-particle mass spectrometry, Atmos. Meas. Tech., 14, 4171–4185, https://doi.org/10.5194/amt-14-4171-2021, 2021.

Peacock, P. M., Zhang, W.-J., and Trimpin, S.: Advances in Ionization for Mass Spectrometry, Anal. Chem., 89, 372–388, https://doi.org/10.1021/acs.analchem.6b04348, 2017.

Wang, G., Ruser, H., Schade, J., Passig, J., Adam, T., Dollinger, G., and Zimmermann, R.: 1D-CNN Network Based Real-Time Aerosol Particle Classification With Single-Particle Mass Spectrometry, IEEE Sens. Lett., 7, 1–4, https://doi.org/10.1109/LSENS.2023.3315554, 2023.

Wenzel, R. J. and Prather, K. A.: Improvements in ion signal reproducibility obtained using a homogeneous laser beam for on-line laser desorption/ionization of single particles, Rapid Commun. Mass Spectrom., 18, 1525–1533, https://doi.org/10.1002/rcm.1509, 2004.

Xiao, Q., Li, M., Liu, H., Fu, M., Deng, F., Lv, Z., Man, H., Jin, X., Liu, S., and He, K.: Characteristics of marine shipping emissions at berth: profiles for particulate matter and volatile organic compounds, Atmos. Chem. Phys., 18, 9527–9545, https://doi.org/10.5194/acp-18-9527-2018, 2018.

Zhai, J., Yu, G., Zhang, J., Shi, S., Yuan, Y., Jiang, S., Xing, C., Cai, B., Zeng, Y., Wang, Y., Zhang, A., Zhang, Y., Fu, T.-M., Zhu, L., Shen, H., Ye, J., Wang, C., Tao, S., Li, M., Zhang, Y., and Yang, X.: Impact of Ship Emissions on Air Quality in the Greater Bay Area in China under the Latest Global Marine Fuel Regulation, Environ. Sci. Technol., 57, 12341–12350, https://doi.org/10.1021/acs.est.3c03950, 2023.